Wetlands Ecol Manage (2024) 32:207–227
https://doi.org/10.1007/s11273-023-09971-y

ORIGINAL PAPER

Using UAV multispectral photography to discriminate plant species in a seep wetland of the Fynbos Biome

Kevin Musungu · Timothy Dube · Julian Smit · Moreblessings Shoko

Received: 7 June 2023 / Accepted: 28 November 2023 / Published online: 6 January 2024

Abstract Wetlands harbour a wide range of vital ecosystems. Hence, mapping wetlands is essential to conserving the ecosystems that depend on them. However, the physical nature of wetlands makes fieldwork difficult and potentially erroneous. This study used multispectral UAV aerial photography to map ten wetland plant species in the Fynbos Biome in the Steenbras Nature Reserve. We developed a methodology that used K-Nearest Neighbour (KNN), Support Vector Machine (SVM), and Random Forest (RF) machine learning algorithms to classify ten wetland plant species using the preselected bands and spectral indices. The study identified Normalized green red difference index (NGRDI), Red Green (RG) index, Green, Log Red Edge (LogRE), Normalized Difference Red-Edge (NDRE), Chlorophyll Index Red-Edge (CIRE), Green Ratio Vegetation Index (GRVI), Normalized Difference Water Index (NDWI), Green Normalized Difference Vegetation Index (GNDVI) and Red as pertinent bands and indices for classifying wetland plant species in the Proteaceae, Iridaceae, Restionaceae, Ericaceae, Asteraceae and Cyperaceae families. The classification had an overall accuracy of 87.4% and kappa accuracy of 0.85. Thus, the findings are pertinent to understanding the spectral characteristics of these endemic species. The study demonstrates the potential for UAV-based remote sensing of these endemic species.

Keywords Fynbos · Wetlands · Unmanned aerial vehicles · Pigments · Indices · Machine learning

Introduction

Wetlands harbour a wide range of biodiversity and play a crucial role in hydrological and biogeochemical cycles (Kingsford et al. 2016). For instance, wetlands improve water quality, attenuate floods, regulate stream flow, trap sediment, sequester carbon, control erosion, and serve as a marine and terrestrial species habitat. Thus, wetlands have the highest value per hectare among ecosystems (Xu et al. 2019). In South Africa, 48% of wetland ecosystems are classified as critically endangered, 12% as endangered and 5% as vulnerable (Job et al. 2018). Over half of the South African wetlands have already been degraded (Dumakude and Graham 2017). Moreover, fine-scale data, such as species occurrence and distribution, has not

K. Musungu · J. Smit
Department of Civil Engineering and Geomatics, Cape Peninsula University of Technology, Cape Town, South Africa

K. Musungu (✉) · M. Shoko
Division of Geomatics, University of Cape Town, Cape Town, South Africa
e-mail: Musunguk@cput.ac.za

T. Dube
Institute of Water Studies, Department of Earth Sciences, University of the Western Cape, Cape Town, South Africa

been captured for most inland South African wetlands (Van Deventer et al. 2018). Yet, identifying wetlands and their functions is essential to understanding, rehabilitating, and conserving wetlands and protecting the ecosystems that depend on them (Rebelo et al. 2009; Bonthuys 2020). The physical indicators for monitoring wetlands include extent and diversity, landscape pattern, hydroperiod and chemical contaminants. The biological indicators include vegetation species composition, greenness and percentage cover (Adamus 1992).

Traditional methods for mapping extent and diversity, such as floristic mapping, require rigorous fieldwork and manual estimation of proportional cover for each species of interest (Sharp and Keddy 1986; Wijana and Setiawan 2020). Additionally, the physical characteristics of wetlands make fieldwork very challenging, expensive and imprecise (Everitt et al. 2002; Hemati et al. 2023). Thus, only small areas can be mapped precisely, and extrapolation could be erroneous (Millar 1973; Harvey and Hill 2001; Morrison et al. 2020; Morrison 2021). Remote sensing technology offers a less intrusive (Rundquist et al. 2001; Lane et al. 2014, 2015) and more scalable approach (Rebelo et al. 2009; Adam et al. 2010; Yan et al. 2017; Moity et al. 2019) for mapping wetland plant species. Also, repeated coverage can facilitate the thorough detection of temporal changes in wetlands (Ramsey Elijah et al. 2009; Sica et al. 2016; Jia et al. 2020; Hasan et al. 2023), although the mapping capability of remote sensing technologies can be hampered by coarse spatial resolution (De Roeck et al. 2007).

Conversely, several characteristics of wetlands make them inherently difficult to monitor remotely. For example, wetlands are generally highly dynamic, and their spectral responses frequently change (Karabulut 2018; Montgomery et al. 2021). Studies have shown that the spectral responses of individual wetland species can vary significantly even within the same growing season (Gallant 2015). Moreover, steep environmental gradients within and around wetlands can result in narrow transition areas between ecological systems that are sometimes smaller than the spatial resolution of most sensors (Harvey and Hill 2001; Adam et al. 2010). Also, sensor resolution can limit understanding of the interactions between different ecological systems, making managing and protecting wetland ecosystems harder.

The advent of low-cost data collection platforms such as Unmanned Aerial Vehicles (UAVs) has made it affordable to gather high-resolution remote sensing data over specific areas at specified times (Tu et al. 2019; Wijesingha 2020; van Blerk et al. 2022). Recent developments in technology and data processing for UAVs have provided novel opportunities to resolve some of the impediments to wetland studies, such as the difficulty of field surveys, coarse satellite resolutions and high costs of piloted aerial photography (Dronova et al. 2021). In fact, UAVs have several advantages over satellites. For instance, UAVs are not affected by cloud cover. Also, UAV payloads are interchangeable, and end-users can control data acquisition parameters such as spatial resolution, frequency of data collection and view angles (Alvarez-Vanhard et al. 2021). On the other hand, UAV data acquisition is affected by wind and precipitation, requires a trained operator, accurate ground control, and it is highly regulated by legislation (Jeanneret and Rambaldi 2016; Stöcker et al. 2017; Assmann et al. 2019) Still, the use if UAVs in wetland studies is gaining traction. A review study found that several UAV-based studies were conducted in the United States, China and Europe with emphasis on riverine and floodplain, mangrove and peatland (Dronova et al. 2021). Only one of the 122 papers reviewed was a South African case study focused on wetland delineation (Boon et al. 2016).

Fifteen papers reviewed by Dronova et al. (2021) focused on vegetation inventory, and most of them utilized Object-based Image Analysis (OBIA) using target characteristics such as canopy diameter, shape, height and distribution pattern. Unlike pixel-based classification methods, OBIA aggregates pixels into spectrally similar objects using segmentation algorithms prior to classifying the objects (Tian et al. 2020). The spatial and textural characteristics of the objects can complement spectral data and improve classification accuracy (Whiteside and Ahmad 2005; Liu and Xia 2010; Giglio et al. 2019; Du et al. 2021). The key drawback with OBIA is the difficulty of choosing segmentation parameters. During segmentation, individual pixels are grouped into segments (objects) based on specific criteria, including the uniformity within each segment, the capacity to distinguish them from neighboring elements (dissimilarity), and the consistency of their shapes (Veljanovski et al. 2011; Cheng and Han 2016). The accuracy of the classification process hinges on the quality of the segmentation process (Veljanovski et al. 2011; Cheng and Han 2016; Gibril et al. 2020). Determining the essential segmentation criteria often involves a process of trial and error, and these criteria can multiply and contradict one another, ultimately leading to either an excessive or insufficient level of segmentation (Liu and Xia 2010; Veljanovski et al. 2011). Moreover, feature selection can sometimes have an adverse effect on the classification process (Ma et al. 2017). Also, the consistency and repeatability of the segmentation and classification processes is still contentious (Veljanovski et al. 2011). In light of these challenges, pixel-based approaches are still more common (Nezami et al. 2020; Allen et al. 2021; Mirmazloumi et al. 2021; van Blerk et al. 2022; Zhu et al. 2022; Windle et al. 2023). Furthermore, some studies have explored both OBIA and pixel-based methods and recommended the latter (Giglio et al. 2019; Abeysinghe et al. 2019).

These include the emerging use of deep learning algorithms in wetland studies (Sun et al. 2021; Higgisson et al. 2021; Yang et al. 2022). Deep learning enables the creation of trainable models that can learn data representations with multiple levels of abstraction (Janiesch et al. 2021). Deep learning possesses a powerful capacity to comprehend intricate training samples and exhibit strong robustness when classifying complex features, like wetland landscapes in remote sensing (RS) images (Jafarzadeh et al. 2022). Some studies have found deep learning algorithms can outperform common shallow learning algorithms (Rezaee et al. 2018; DeLancey et al. 2019) and others have found contradicting results (Islam et al. 2023). However, deep learning is most pertinent when dealing with large, high dimensional data. Shallow machine learning algorithms can produce better results than deep learning algorithms when utilizing low-dimensional and low training data (Janiesch et al. 2021). The popular shallow learning non-parametric machine learning classifiers include Random Forest (RF), Support Vector Machines (SVM), and K Nearest Neighbor (KNN) (Belgiu and Drăguţ 2016; Chirici et al. 2016; Sheykhmousa et al. 2020). KNN is a non-parametric machine learning algorithm that classifies individual data points based on proximity to data points with known classes (Mucherino et al. 2009a). The algorithm compares a number (k) of the closest training data points in feature space to a new data point and then classifies the individual data point based on the most common class among the k-nearest neighbours. Support Vector Machines utilize an optimal line of separation, a hyperplane, to classify data points by maximizing the margin between the class boundaries (Mucherino et al. 2009b). SVMs are popular because of their capacity to control the trade-off between maximizing the margin and classification errors. Random Forest is an ensemble learning algorithm aggregating multiple decision trees to predict the most likely class of an individual point. Each decision tree in the Random Forest is trained on a randomly selected subset of the training data and a random subset of the features. This process, called bagging, helps to reduce overfitting by increasing the diversity of the trees in the forest (Breiman 1996).

This pilot study aimed to develop a methodology to map the significant plant species in a seep wetland using UAV aerial photography and establish a baseline to monitor changes. To our knowledge, this is the first study to map several seep wetland species in the Fynbos Biome simultaneously using UAV multispectral data.

Materials and methods

Study area

The study site is south of the upper Steenbras dam in the Steenbras Nature Reserve in Cape Town. The Steenbras Nature Reserve is located between Gordon's Bay and Rooi-Els, within the greater Kogelberg Biosphere Reserve. The Kogelberg area is called 'the heart of the fynbos' because the reserve has several plant families and more than 1650 plant species (Wittridge 2011). Two-thirds of these species are endemic to this region. The Steenbras Catchment area was also identified as a pilot site for water abstraction from the Table Mountain Group Aquifer (TMGA) (Wiese et al. 2020). The yield from the first phase of the TMGA project is predicted to be 10 million liters per day, which will be channeled into the Steenbras Dam to complement the Cape's bulk water supply and boost water resilience. However, boreholes should be drilled in ecologically acceptable areas and operated responsibly (Blake et al. 2021). This wetland site was chosen for monitoring because of its proximity to the City of Cape Town's groundwater drilling sites in the

Steenbras reserve. It is an inland seep wetland located within the Southern Folded Mountains ecoregion (Ollis et al. 2013) and has a variety of plant species spread over an area of approximately 1300 square meters (See Fig. 1). It is located in close proximity to a valley-bottom stream.

As previously mentioned, this pilot phase aimed to develop a methodology to map the significant plant species in the wetland using UAV aerial photography and establish a baseline to monitor any effects of water abstraction in the TMGA may have on the wetland plant species. The key plant families and species in the wetland are Proteaceae (*Berzelia alopecuroides*, *Berzelia lanuginose)*, Iridaceae *(Borbatia gladiata)*, Restionaceae (*Elegia mucronata, Platycaulos compressus*, *Restio dispar)*, Ericaceae (*Erica campanularis*, *Erica intervallaris* and *Erica serrata*), Asteraceae (*Grubbia rosmarinifolia*), and Cyperaceae (*Tetraria Thermalis*).

Data collection

A Real-Time Kinematic (RTK) survey was undertaken using Global navigation satellite systems (GNSS) to establish coordinates of ground control points (GCPs). The GCPs were surveyed on the periphery of the block (Fig. 2). Studies have shown that GCPs placed around the periphery of the site can minimize planimetric errors (Martínez-Carricondo et al. 2018; Ulvi 2021). It is recommended to have a minimum of 4 to 5 Ground Control Points (GCPs) for every square kilometer (Ferrer-González et al. 2020). In total, six GCPs were surveyed from base station STEENBSE and used in the study. Then, a DJI Phantom 3 Professional (DJI-Innovations Inc., Shenzhen, China) was used with a Parrot Sequoia multispectral camera. The Phantom 3 had been modified such that the onboard camera had been removed and replaced with the Parrot Sequoia.

The Parrot Sequoia has four monochrome sensors with a global shutter focal length of 3.98 mm. The sensors correspond to four bands, namely Green (530–570 nm), Red (640–680 nm), Red Edge (730–740 nm) and Near Infrared (770–810 nm). The camera also has an RGB sensor with a rolling shutter and a focal length of 4.88 mm. The Sequoia has an irradiance (sunshine) sensor above the drone that is connected during data capture to facilitate the processing of at-sensor reflectance (Padró et al. 2019). A Micasense calibration reflectance panel was also used to process radiometrically corrected reflectance maps (Fig. 3d).

The aerial photographs were captured on 4th October 2018. Plastic ground control targets were placed over the GCPs such that the center of each target coincided with the GCP. The targets were black

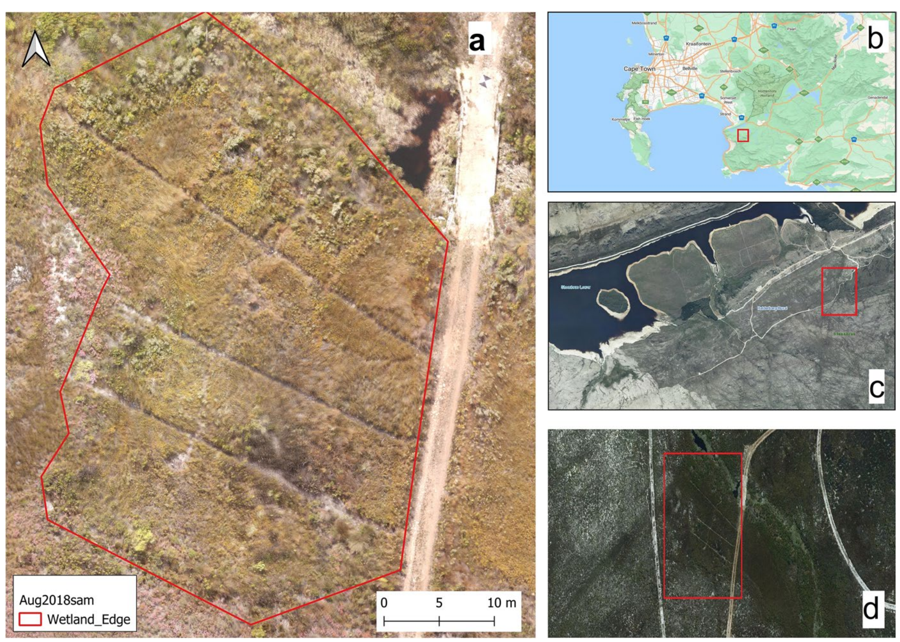

Fig. 1 **a** Extent of study area. **b** Location of site in Western Cape Province. **c** Location of study area in Steenbras reserve. **d** Location of wetland area relative to the valley-bottom stream

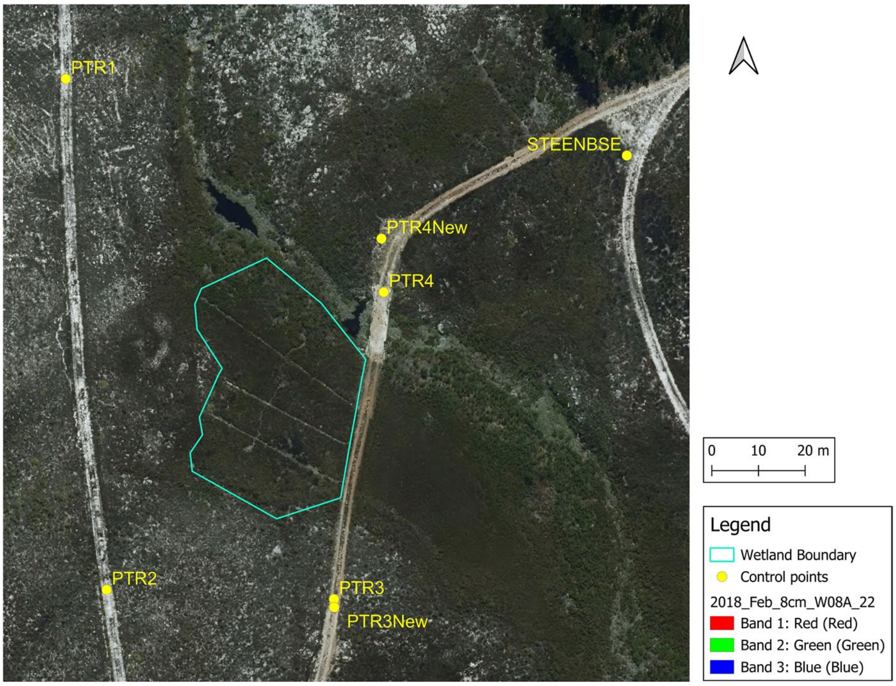

Fig. 2 Spatial distribution of GCPs relative to the study area

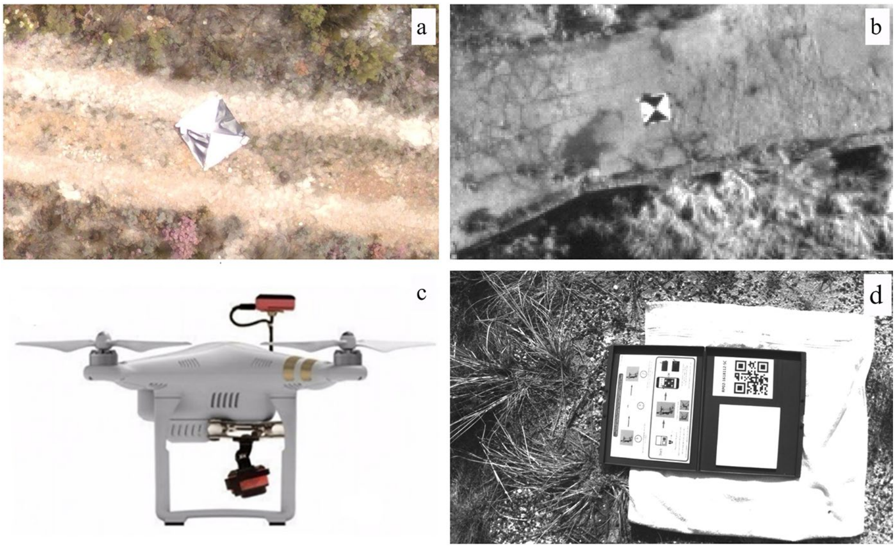

Fig. 3 **a** Target placed over GCP; **b** View of target in a red edge photo; **c** DJI Phantom 3 with Parrot Sequoia payload and irradiance sensor above UAV (Padró et al. 2019); **d** A pre-flight photo of the radiometric calibration panel used for radiometric processing

and white mats measuring 1 m by 1 m in dimension (Fig. 3a and b). The flight plan was designed in the Atlas Flight application. The flight parameters were a height above ground of 25 m, an overlap of 80%, and a flight speed of 5 m/s. In addition, all the sensors (RGB, Green, Red, Near Infrared and Red Edge) were activated, and the data collection started at midday. The drone was held over a Micasense calibration reflectance panel at the start and the end of the flight in order to take calibration photos in each band (See Fig. 3d).

Data processing

Initial processing of UAV aerial photography

All the RGB aerial photography processing was done in Pix4Dmapper (Pix4D SA, Lausanne, Switzerland).

The first step involved computing 10,000 key points on the images to create a sparse point cloud. The coordinates of the surveyed GCPs were then added to the project, and the next step involved creating a densified point to create orthophotos and an orthomosaic with a resolution of 3 cm per pixel.

The Parrot Sequoia multispectral photos were processed similarly, except each band was radiometrically calibrated before the orthophotos were created. The calibration was done using the one-point calibration plus sunshine sensor method (Poncet et al. 2019). The calibration involved using average reflectance factor values provided by the camera manufacturers with the Micasense reflectance calibration panels. The average reflectance factors were recorded in Pix4D Mapper for each calibration photo based on the factors recommended for each band. The Pix4D software then calibrated the images during data processing based on the differences between the observed values and the actual reflectance values recorded at the reflectance target for each band in the camera. Several spectral indices were also calculated in the final step of the processing (See Table 1).

Feature selection

The processed orthomosaics were layer stacked along with the calculated vegetation indices described in the preceding section. Several studies reported improvements in classifying plant species in layer-stacked images after including spectral indices (Abeysinghe et al. 2019; Bhatnagar et al. 2020; Jin et al. 2016; Mudereri et al. 2020). During the survey of the GCPs, 211 points were surveyed within the wetland, and the description of the plant species at those points was simultaneously recorded. An additional 257 polygons were digitized in Quantum GIS (QGIS) based on the locations of the GNSS surveyed points to ensure sufficient samples for classification and accuracy assessment. A point-in-polygon algorithm in QGIS was

Table 1 Eighteen vegetation indices (VIs) were derived from multispectral images in this study

Vegetation indices	Formula	References
Enhanced Vegetation Index 2 (EVI2)	2.5 x (N-R)/(1 + N+(2.4 x R)	(Jiang et al. 2008)
Normalized Difference Vegetation Index (NDVI)	(N-R)/(N + R)	(Rouse et al. 1974)
Green Normalized Difference Vegetation Index (GNDVI)	(N-G)/(N + G)	(Louhaichi et al. 2001)
Green Ratio Vegetation Index (GRVI)	N/G	(Sripada et al. 2005)
Transformed DVI (TDVI)	$\sqrt{}$[0.5+(N-R)/(N + R)]	(Bannari et al. 2002)
Normalized Green–Red Difference Index (NGRDI)	(G-R)/(G + R)	(Tucker 1979)
Non-Linear Index (NLI)	(N^2-R)/(N^2 + R)	(Goel and Qin 1994)
Modified Soil Adjusted Vegetation Index 2 (MSAVI2)	0.5x[2xN + 1- $\sqrt{}$((2 x N + 1)^2-8x(N-R)]	(Richardson and Wiegand 1977)
Normalized Difference Water Index (NDWI)	(G-N)/(G + N)	(McFeeters 1996)
Chlorophyll Index Red Edge (CIRE)	(N/RE)-1	(Gitelson 2005)
Normalized Difference Red Edge (NDRE)	(N-RE)/(N + RE)	(Boiarskii and Hasegawa 2019)
Renormalized Difference Vegetation Index (RDVI)	(N-R)/$\sqrt{}$(N + R)	(Roujean and Breon 1995)
Modified Simple Ratio (MSR)	(N/R-1)/$\sqrt{}$(N/R + 1)	(Chen 1996)
Green Soil Adjusted Vegetation Index (GSAVI)	1.5x(N-G)/(N + G + 0.5)	(Sripada et al. 2005)
Enhanced NDVI index (ENDVI)	((N + G) -2xR)/ ((N + G) + 2xR)	(Rasmussen et al. 2016)
Log Red (LogR)	logR	This study
Log Red Edge (LogRE)	logRE	This study
Red Green Vegetation Index (RG)	2R-G	This study

N Near Infrared, *R* Red, *G* Green and *RE* Red Edge used to randomly fit points in the polygons. The criteria were that up to 20 points could be fitted in a polygon depending on the polygon size but the point spacing had to be at least 5 cm to avoid having two points overlaying the same pixel. In total, 8466 points were created. A shapefile of the points was overlaid on the layer stack consisting of the multispectral bands and the vegetation indices. A shapefile is a data format of Geographic information systems (GIS)(Elliott 2014). Reflectance values were sampled where the GNSS surveyed positions intersected the layer stack, and those values were exported to a spreadsheet. The spreadsheet consisted of 8466 data rows, with one column containing the class (plant species) data and several columns corresponding to the sampled reflectance values for that class in the spectral bands and vegetation indices. The feature selection was implemented using Recursive Feature Elimination (RFE) in R based on the *Caret* and *Random Forest* libraries. RFE aims to identify the essential features in a dataset by iteratively removing less critical features and refitting the model until a desired number of features is obtained (Demarchi et al. 2020; Ramezan 2022). The importance of a variable can be determined by examining the rankings assigned to each variable during the RFE process. Variables that are consistently ranked high throughout the iterations are considered to be more important, while those that are consistently ranked low are considered to be less important (R.-C. Chen et al. 2020). In order to assess the efficiency of the feature selection, two image layer stacks were created prior to classification. One contained only the original bands and the other contained the key bands and indices selected by RFE.

Finetuning parameters

One of the crucial steps in classification with machine learning is tuning the optimum hyperparameters of the machine learning classifiers. These include, for instance, the best values for γ and C for the radial basis function kernel in Support Vector Machines, where γ denotes the free parameter of the radial basis function, and C is the parameter that allows a trade-off between the training error and the complexity of the model. For random forest classifiers, one must optimize the number of trees in the forest (best n_estimators) and the maximum number of features considered for splitting a node (best max_features). Tuning such hyperparameters involves testing different combinations of hyperparameter values and selecting the best performance (Kranjčić and Medak 2020; Thanh Noi and Kappas 2017).

The hyperparameters used in this study were determined statistically and used for classification. Fifteen-centimeter buffers were created around the GNSS shapefile points in QGIS in order to create polygons. The new polygon shapefile was merged with the digitized polygons to make a new shapefile containing the GNSS surveyed locations and the digitized polygons. Seventy per cent of the polygons in the new shapefile were used as classification samples, and the other 30% was retained for validation. The classification samples were used to determine the hyperparameters for Random Forest, Support Vector Machine and K Nearest Neighbour using stratified k-fold cross-validation. The Dzetsaka plugin (Karasiak 2016), a Quantum GIS (QGIS) plugin that uses Python Scikit-learn (Pedregosa et al. 2011), was used for the cross-validation. This approach randomly splits the observations into k groups, also called folds, of approximately equal size. The first fold is then treated as a validation dataset, and the classifier is trained on the remaining $k-1$ folds. The Mean Square Error (MSE) is calculated on the validation fold. This process is repeated k times, and the MSE is averaged to get the cross-validation estimates. In the stratified cross-validation approach, the folds are made by preserving the same percentage of training samples for each information class.

In this study, the classification dataset was split into 5 groups (i.e., $k=5$) and 80% of the samples from each class were used for training and the other 20% for validation. The best hyperparameters were identified by scripting a grid search in the Dzetsaka plugin.

Classification

All three machine learning classifiers, namely, Random Forest (RF), Support Vector Machines (SVM), and K Nearest Neighbour (KNN), were used in the classification. Two image layer stacks were classified: one with only the original bands and the other with the ten best bands and indices (See Fig. 4). In both instances, the classification was optimized with finetuned hyperparameters. The results are presented in the forthcoming section. The validation

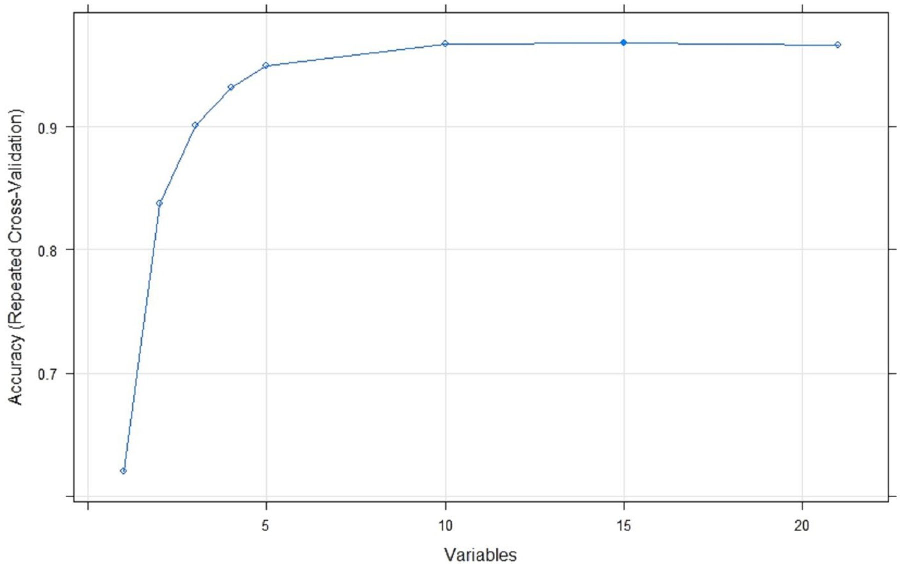

Fig. 4 Graph showing classification model accuracy plotted against number of features

dataset comprising 30% of the samples was used to calculate the Overall Accuracy (OA) and the Kappa hat coefficient (k). The equations for calculating overall accuracy and kappa are shown below.

$$OA = \frac{number\ of\ \ correctly\ \ classified\ \ pixels}{total\ number\ \ of\ pixels} \tag{1}$$

$$k = \frac{N\sum_{i=1}^{r} x_{ii} - \sum_{i=1}^{r}\left(x_{i+1} \times x_{+i}\right)}{N^2 - \sum_{i=1}^{r}(x_{i+} \times x_{+i})} \tag{2}$$

where r = the number of rows and columns in the error matrix, x_{ii} = the number of observations in row i and column i, x_i+ = the marginal sum of row i, x_{+i} = the marginal sum of column i, and N = the total number of observations.

User and producer accuracies were also calculated. Producer accuracies are the probability that a land cover class is classified as such (Story and Congalton 1986). The user accuracy represents the probability that the predicted class on the map is present on the ground or to what extent the other classes may have been misclassified as the class in question (Congalton et al. 1983; Patel and Kaushal 2010). Lastly, the degree of agreement or consensus between the classifiers was determined by comparing the spatial overlap of the class distributions in the classification images (Mas et al. 2022). The degree of agreement was calculated per classifier as well as per class.

Results

Feature selection

The RFE results showed that using fifteen features instead of twenty-two would produce the best accuracy results (Fig. 4). However, the cross-validation accuracy assessment of the models developed using RFE when using ten, fifteen and all variables were very similar. The kappa values were 0.960, 0.961 and 0.959, respectively. Thus, only the top ten features, namely NGRDI, RG, Green, LogRE, NDRE, CIRE, GRVI, NDWI, GNDVI and Red were subsequently used to classify the plant species.

Figure 5 below shows the relative feature importance of the top fifteen features selected during the RFE feature selection.

Classification maps

Figure 6 shows the spatial distributions of the plant species in the wetland. The plant species thrive in different parts of the wetland based on the degree of soil wetness. The three classifiers generally showed a similar distribution of the species.

Classification statistics

Figure 7 shows the accuracy statistics for each classifier for both layer stacks (one with original bands

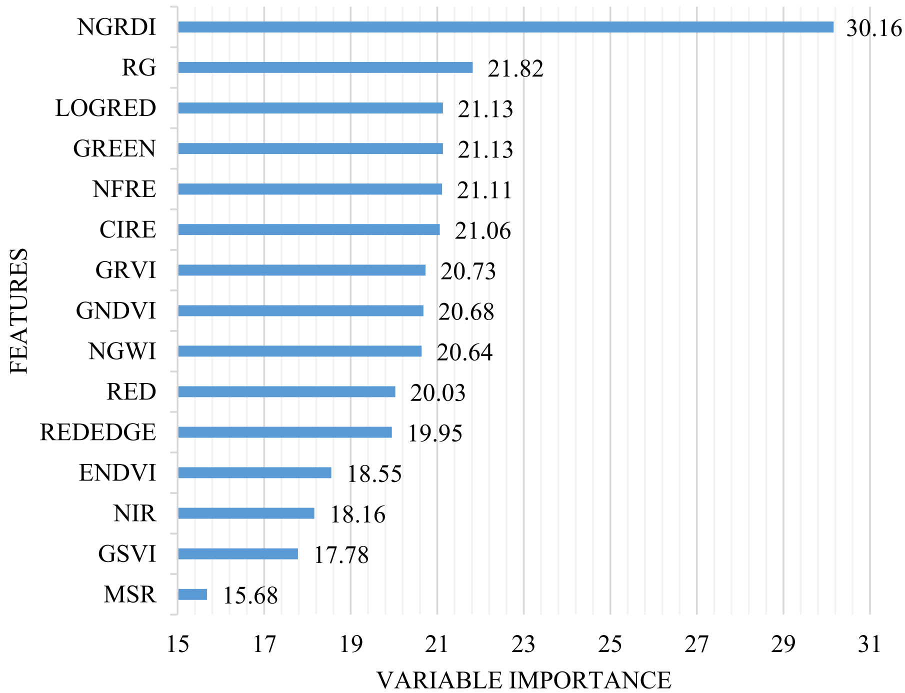

Fig. 5 Showing the variable importance of the bands and indices

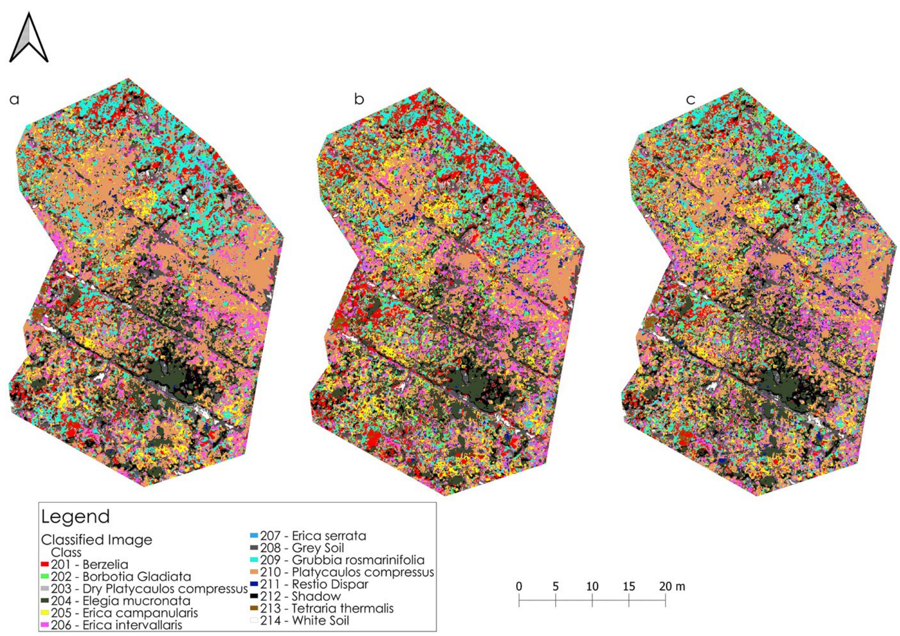

Fig. 6 Classified images **a** Random Forest, **b** SVM, **c** KNN for layer stack with indices

and the other with RFE selected bands and indices). The columns with the suffix 'WI' indicate the datasets after feature selection. The table after that (Table 2) shows classification accuracies per class.

The best classifier was Random Forest, with an overall accuracy of 87% and kappa hat value of 0.85. The overall classification accuracy was 4% better than the results from Support Vector Machines and 2%

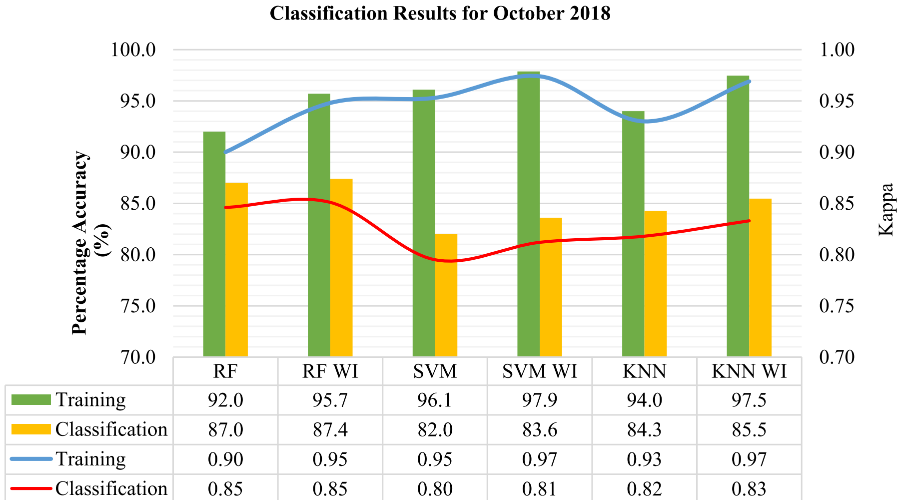

Fig. 7 Overall model training and classification accuracies for all classifiers

Table 2 Classification accuracies per class for each classifier

Classifier	Random Forest			Support Vector Machines			K Nearest Neighbour		
Class	PA [%]	UA [%]	K	PA [%]	UA [%]	K	PA [%]	UA [%]	K
B	85.05	66.73	0.63	89.65	66.37	0.62	85.82	72.22	0.69
BG	83.8	85.25	0.85	85.3	75.79	0.75	89.03	74.51	0.74
DPC	87.99	92.9	0.93	78.51	94.57	0.94	77.93	96.26	0.96
EM	94.74	92.83	0.92	96.02	90.52	0.89	93.58	92.27	0.91
EC	88.25	73.24	0.72	87.86	72.86	0.7	90.05	74.19	0.72
EI	89.71	83.51	0.82	84.47	76.38	0.74	88.91	76.49	0.74
ES	35.36	57.5	0.57	42.05	73.68	0.73	53.11	69.57	0.69
GS	91.75	95.23	0.95	88.94	94.29	0.94	88.81	91.48	0.91
GR	74.78	90.21	0.88	67.63	93.04	0.92	74.6	92.96	0.92
PC	93.04	96.93	0.96	85.82	96.64	0.96	86.36	96.28	0.95
RD	47.25	60.71	0.6	46.54	53.06	0.52	65.93	57.43	0.56
S	96.1	89.44	0.89	94.78	91.04	0.91	96.66	89.71	0.89
TT	87.18	82.67	0.83	96.33	80.85	0.81	76.18	74.5	0.74
WS	85.26	57.11	0.57	41.17	64.81	0.65	72.85	69.28	0.69

OA Overall accuracy, *K* Kappa. *PA* Producer accuracy and *UA* User Accuracy

better than K Nearest Number. The producer accuracies ranged between 84% and 96%. Figure 7 also shows that the overall training accuracies and kappa hat values were generally good for all the classifiers. Figures 8 and 9 are graphical representations of Table 2.

Classification accuracy per class

Classification accuracies differed across the plant species (Table 2). The descriptions of the acronyms in the table are as follows: B (*Berzelia*), BG (*Borbotia Gladiata*), DPC (*Dry* or *Dead Platycaulos Compressus*), EM (*Elegia Mucronata*), EC (*Erica Campanularis*), EI (*Erica Intervallaris*), ES (*Erica Serrata*), GS (Grey Soil), GR (*Grubbia Rosmarinifolia*), PC (*Platycaulos Compressus*), RD (*Restio Dispar*), S (Shadow), TT (*Tetraria Thermalis*) and WS represents White Soil. The accuracies vary with each class and classifier.

The *Berzelias, Erica Serrata* and *Restio Dispar* had the lowest classification accuracies with Kappa hat values of 0.63, 0.57 and 0.60, respectively. The *Erica Serrata* was classified better using the Support

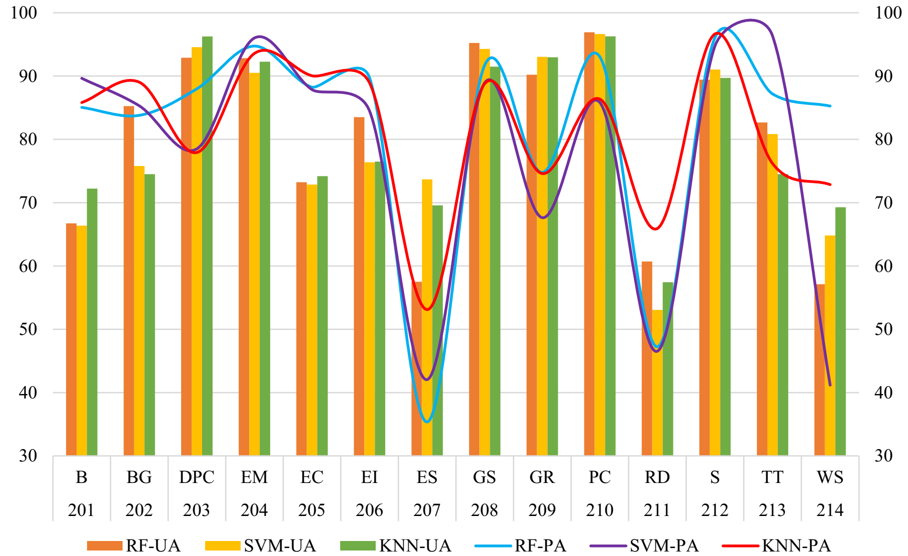

Fig. 8 Graph showing producer and user accuracies per class

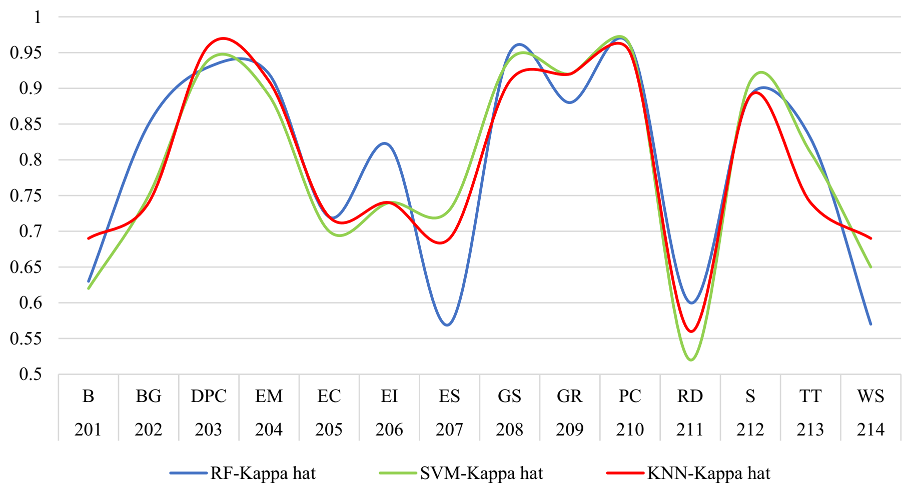

Fig. 9 Graph showing kappa hat values per class

Vector Machines classifier with a Kappa hat accuracy of 0.73. The *Berzelias* were classified best using the K Nearest Neighbour classifier. Conversely, the taller, more dominant species, *Grubbia Rosmarinifolia*, *Platycaulos Compressus* and *Elegia Mucronata* were classified well with kappa hat values of 0.88, 0.96 and 0.92, respectively. The *Borbotia Gladiata* and *Tetraria Thermalis* clusters are less than half a meter in height but also had acceptable classification results with kappa hat values of 0.85 and 0.83, respectively. In contrast to the *Erica Serrata*, the *Erica Campanularis* and *Erica Intervallaris* showed good accuracies of 0.72 and 0.82, respectively. K Nearest Neighbor presented the best producer accuracies for *Erica Serrata* and *Restio Dispar*. K Nearest neighbour performed well classifying the Erica family of flowering plants and the small clusters of *Borbotia Gladiata*, *Dead Platycaulos Compressus* and *Restio Dispar*.

However, Random Forest generally had comparatively good user accuracy statistics. The user accuracy is a measure of reliability of the classification to the user (Rwanga and Ndambuki 2017). It is the likelihood that the classification result actually represents that category on the ground (Story and Congalton 1986). Though the Random Forest classifier wrongly classified some pixels as per the producer accuracy statistics (Fig. 8), it generally produced the most user-reliable classification of the individual classes.

Nearest Neighbor presented the best producer accuracies for both the *Erica Serrata* and *Restio Dispar*. K Nearest neighbour performed well classifying the Erica family of flowering plants and the small clusters of *Borbotia Gladiata*, *Dead Platycaulos Compressus* and *Restio Dispar*. However, Random Forest generally had comparatively good user accuracy statistics. Thus, although the Random Forest classifier wrongly classified some pixels as per the producer accuracy statistics (Fig. 8), it generally produced the most user-reliable classification of the individual classes.

Degree of agreement between classifications

Table 3 shows the degree of similarity between the different classification maps. The descriptions of the acronyms in the table are as follows: B (*Berzelia*), BG (*Borbotia Gladiata*), DPC (*Dry* or *Dead Platycaulos Compressus*), EM (*Elegia Mucronata*), EC (*Erica Campanularis*), EI (*Erica Intervallaris*), ES (*Erica Serrata*), GS (Grey Soil), GR (*Grubbia Rosmarinifolia*), PC (*Platycaulos Compressus*), RD (*Restio Dispar*), S (Shadow), TT (*Tetraria Thermalis*) and WS represents White Soil.

The best agreement across all classifiers was for *Borbotia Gladiata, Dead Platycaulos Compressus, Elegia Mucronata, Erica Campanularis* and *Tetraria Thermalis*. There was 70.48% overall agreement (and kappa of 0.66) between the Random Forest and K nearest neighbor results. Among the plants, the highest agreement was achieved when mapping *Tetraria Thermalis, Restio Dispar, Elegia Mucronata* and *Borbotia Gladiata* respectively. Despite an overall agreement of almost 65.77% (and kappa of 0.60), there was poor agreement between the classification outputs of Random Forest and Support Vector machines for *Platycaulos Compressus, Erica Serrata and Restio Dispar.*

Lastly, there was fairly good agreement between K Nearest neighbor and Support vector Machines (70.51% and kappa of 0.66). The highest consensus for the two classifiers was found for *Elegia Mucronata*, *Grubbia Rosmarinifolia* and *Berzelia* and poor agreement was found for the classification of *Erica Serrata* and *Restio Dispar*.

Discussion

This study sought to ascertain the UAV multispectral aerial photography capacity to remotely map several seep wetland plant species in the Fynbos Biome. The key plant families and species explored were Proteaceae (*Berzelia alopecuroides*, *Berzelia lanuginose)*, Iridaceae *(Borbatia gladiata)*, Restionaceae (*Elegia mucronata, Platycaulos compressus*, *Restio dispar)*, Ericaceae (*Erica campanularis*, *Erica intervallaris* and *Erica serrata*), Asteraceae (*Grubbia rosmarinifolia*), and Cyperaceae (*Tetraria Thermalis*). The study used three machine learning algorithms, namely, Random Forest (RF), Support Vector Machines (SVM), and K Nearest Neighbor (KNN). The hyperparameters for all three classifiers were finetuned to optimize the classification (Duncan et al. 2023; Kuradusenge et al. 2023). The classification was done on a dataset of critical spectral bands and

Table 3 Agreement between the classification results of the different classifiers

RF and KNN - Overall Agreement [%] = 70.48 Kappa hat = 0.66

ClassID	201	202	203	204	205	206	207	208	209	210	211	212	213	214
Classes	B	BG	DPC	EM	EC	EI	ES	GS	GR	PC	RD	S	TT	WS
Kappa	0.61	0.73	0.65	0.74	0.7	0.59	0.59	0.74	0.63	0.6	0.81	0.79	0.83	0.76

RF and SVM - Overall Agreement [%] = 65.77 Kappa hat = 0.60

ClassID	201	202	203	204	205	206	207	208	209	210	211	212	213	214
Classes	B	BG	DPC	EM	EC	EI	ES	GS	GR	PC	RD	S	TT	WS
Kappa	0.61	0.74	0.59	0.73	0.69	0.64	0.51	0.67	0.62	0.48	0.49	0.61	0.74	0.65

KNN and SVM - Overall Agreement [%] = 70.51 Kappa hat = 0.66

ClassID	201	202	203	204	205	206	207	208	209	210	211	212	213	214
Classes	B	BG	DPC	EM	EC	EI	ES	GS	GR	PC	RD	S	TT	WS
Kappa	0.72	0.65	0.60	0.78	0.67	0.64	0.43	0.74	0.72	0.61	0.42	0.58	0.66	0.68

indices selected based on their capacity to optimize the classification process. The findings indicated that by utilizing the RFE-chosen variables, accuracy of the classification training model increased by as much as 3.7%, while the overall accuracy of the classification improved by up to 1.6%. The classification maps showed the spatial distribution of the wetland species in the study area.

Feature selection

Studies have shown that vegetation indices (VIs) can highlight phenological differences and improve the potential for classification (Doughty and Cavanaugh 2019; Ma et al. 2019; Zhuo et al. 2022). Conversely, incorporating VIs before classification increases the dimensionality of multispectral data. Having many features can cause a learning model to overfit and increase the computational cost of data processing. This problem can be mitigated by either feature extraction or feature selection (Jovic et al. 2015; Tang et al. 2014). In feature extraction, the original features are transformed into a new set that retains the more meaningful information from the original collection (Jovic et al. 2015; Tang et al. 2014). Remote Sensing studies (Arun 2022; Avola et al. 2019; Nikolakopoulos et al. 2004) have used feature extraction techniques such as Principal Component Analysis (PCA), Linear Discriminant Analysis (LDA) and Canonical Correlation Analysis (CCA) to reduce data dimensionality. The alternative approach, feature selection, extracts a small subset of features from the original set of features without any transformation (Jovic et al. 2015; Tang et al. 2014). Features are ranked from strongly relevant to redundant, and feature selection aims to capitalize on relevance and diminish redundancy (Jovic et al. 2015). The feature selection methods are broadly categorized as filter, wrapper, embedded, and hybrid. Filter methods select features by assessing their performance independently of data modelling algorithms. Wrapper methods perform better than filter methods because the feature subsets are evaluated by how well they improve the performance of a modelling algorithm (Jovic et al. 2015).

This study used Recursive Feature Elimination (RFE) for feature selection. RFE is a wrapper feature selection method frequently used with random forest and support vector machines (Demarchi et al. 2020; Poona et al. 2016). RFE starts by testing the complete feature set and computing each component's importance score. Then, the least important features are iteratively removed as the model is reassembled, and an importance score is recalculated until the user-defined number of subsets is reached. This study used the RFE to create ten subsets to identify the best fifteen features for classification. The process was repeated five times. Eighteen vegetation indices were assessed along with the four multispectral bands (n = 22).

The results showed that the model's accuracy peaked at 15 features out of 22. However, the accuracies when using ten, fifteen and all features were very similar, with kappa hat values of 0.960, 0.961 and 0.959, respectively. The features added after the first ten did not significantly improve the accuracy of the classification model. Consequently, 60% of the features were discarded before classification at an insignificant cost to classification accuracy. The retained indices were NGRDI, RG, LogRE, NDRE, CIRE, GRVI, NDWI and GNDV. The NGRDI had a significantly higher importance score than the other features.

The wetland vegetation properties

This study found that NGRDI, RG, Green, LogRE, NDRE, CIRE, GRVI, NDWI, GNDVI and Red were essential for classifying wetland vegetation. Of these variables, the Normalized Green–Red Difference Index (NGRDI) was significantly more important than the rest. NGRDI leverages differences in the reflectance of the Green and Red bands (Gitelson et al. 2002). Studies have also shown that leaf pigments (chlorophyll, carotenoids and anthocyanins) influence the interaction of vegetation with the visible portion of electromagnetic radiation (Gausman 1977; Govender et al. 2009). The absorbance of the red band is based primarily on chlorophyll content, whilst the absorbance of the green band is based on both chlorophylls and anthocyanins (Gitelson 2011).

Consequently, NGRDI can leverage differences in reflectance of the red portion of the electromagnetic spectrum and highlight vitality in vegetation (Song and Park 2020). Notably, the Red Green Vegetation Index (RG) tested in this study also exploited the reflectance in the Green and Red bands and was the second most crucial variable. Lastly, the Green-Red Vegetation Index (GRVI) is highly sensitive to chlorophyll (Duncan et al. 2023; Yang et al. 2017) and the Green Ratio Vegetation Index (GRVI), which is mathematically similar to the modified anthocyanin index (mACI) is sensitive to anthocyanins(Gitelson 2011; Motohka et al. 2010).

NGRDI has also been correlated with biomass and nitrogen content (Choudhary et al. 2021; Elazab et al. 2016; Hunt et al. 2005; Jannoura et al. 2015; Li et al. 2016; Smigaj et al. 2019) Biomass, chlorophyll concentration and leaf water content are the most significant biophysical and biochemical properties that characterize wetland vegetation (Adam et al. 2010; Mishra 2020). Vegetation biomass is typically a proxy for local carbon storage, wetland health, and vulnerability to human activity and environmental or climate change (Doughty and Cavanaugh 2019; Han et al. 2019; Klemas 2013; Sun et al. 2021). Nitrogen is an essential component of chlorophyll (Bassi et al. 2018; Wang et al. 2014). Thus, the results suggest that there could be significant differences between the chlorophyll content and biomass in the study area to warrant a high performance of NGRDI.

Leaf water content is frequently estimated using the near-infrared to shortwave portions of the electromagnetic spectrum (Govender et al. 2009). However, there is a correlation between leaf water and chlorophyll activity and reflectance of the red-edge part of the spectrum (Ndlovu et al. 2021) Thus, other than NDWI, red-edge indices such as NDRE, GNDVI and CIRE indices have been proposed as water-sensitive vegetation indices (Ndlovu et al. 2021; Yang et al. 2017) Indices can help highlight different vegetation features across various plants, plant concentrations and stages of growth (Boiarskii and Hasegawa 2019).

Classification statistics

Three classifiers were used to classify two datasets. One dataset contained only the original spectral bands, and the other included the bands and spectral indices selected during the RFE process. The results showed that the use of the chosen variables improved the out-of-bag accuracy of the classification training model by up to 3.7% for Random Forest (RF), 1.8% for Support Vector Machines (SVM) and 3.5% for K nearest Neighbour (KNN). In addition, the overall accuracy of the classifications increased by 0.4% (RF), 1.6% (SVM) and 1.2% for K Nearest Neighbour (KNN). Overall, RF had the best classification statistics with an overall accuracy of 87.4% and kappa accuracy of 0.85. KNN had an overall accuracy of 85.3% and kappa accuracy of 0.83; SVM had an overall accuracy of 83.6%; and kappa accuracy of 0.81.

The RF classification determined that *Platycaulos Compressus* was the best classified plant species, followed by the *Elegia Mucronata* and the *Dead Platycaulos Compressus*. All three classes had kappa accuracies of more than 0.9 and less than 10% commission error. The *Grubbia Rosmarinifolia*, *Borbotia Gladiata*, *Erica Intervallaris* and *Tetraria Thermalis* had kappa accuracies of 0.88, 0.85, 0.82 and 0.83. Of these four species, *Grubbia Rosmarinifolia* had the highest producer accuracy of 74.78%, indicating the omission of 25.22% of the species in the final map. In contrast, the user accuracy was 90.21%, suggesting that only 9.79% of the other species were misclassified as *Grubbia Rosmarinifolia*.

The poorly classified species included *Berzelia* (kappa of 0.63), *Restio Dispar (*kappa of 0.56*) and Erica Serrata* (kappa of 0.57). They were generally classified well, with a producer accuracy of 85.05% and low omission error (14.95%). However, the user accuracy of 66.73% suggests the species was overestimated by 33.27%. The KNN classification of the same species only overestimated the species by 27.78%. The *Erica Serrata*, and *Restio Dispar* had the poorest classification statistics. The classification results of *Restio Dispar* indicate that more than 50% of the species were omitted and 39.29% of the classified pixels belonged to other classes. However, it must be noted that *Restio Dispar*, which grew in individual tufts, was also one of the least represented species in the wetland. The *Erica Serrata* was classified with a producer accuracy of 35.36% and a user accuracy of 57.50%. This result means that more than half of the class was omitted, and 42.5% of the class is erroneous. Like *Restio Dispar*, the *Erica Serrata* also occurred in patches and small clusters west of the wetland. The SVM and KNN classifiers performed better than RF in classifying *Erica Serrata*, with 27% and 31% commission errors, respectively. Studies suggest small patch size and plant density can significantly impact classification accuracy (Adam et al. 2010; Duncan et al. 2023). In addition, machine learning classifiers generally require many samples for a good classification (Duncan et al. 2023). The classification accuracies of *Berzelia*, *Restio Dispar* and *Erica Serrata* could be improved by collecting the data in a different season since the spectral signature of wetland species can be affected by different seasons and illumination (Adam et al. 2010; Gallant 2015).

Table 3 shows the degree of agreement between the classifiers. The assessment of classifier agreement revealed strong consensus among classifiers when it came to classifying *Borbotia Gladiata*, *Dead Platycaulos Compressus*, *Elegia Mucronata*, *Erica Campanularis*, *Tetraria Thermalis*, and bareground. However, there was notably less agreement when classifying *Restio Dispar* and *Erica Serrata*, particularly because these species exhibited patchy distribution within the wetland. Remarkably, the Random Forest classifier and K Nearest Neighbour exhibited the highest similarity in classifying these two challenging classes. This observation suggests that these classifiers may demonstrate greater robustness in classifying vegetation types when confronted with limited sample data.

The spatial distribution of the plant species

This paper aimed to map several seep wetland plant species remotely. The study findings showed that the distributions of the dominant plant species in the wetland can be depicted. The plants were found to be clustered in different areas of the wetland. *Grubbia Rosmarinifolia* and *Platycaulos Compressus* were the most prevalent species in the northern portion of the wetland. That area is also the wettest portion of the wetland.

Erica Campanularis and *Erica Intervallaris* thrived in both the wettest portions of the wetland to the North and the drier parts of the wetland to the West and South. *Erica Serrata* was spread around the drier portions of the wetland in small clusters. *Elegia Mucronata* was found to coexist with *Berzelia Lanuginosa* and *Berzelia Alopecuroides*, particularly in less water-logged soils around the transect line at the centre of the wetland. That portion of the wetland is seasonally wet. *Borbotia Gladiata*, *Restio Dispar* and *Tetraria Thermalis* were tiny clusters in the dry parts of the wetland adjacent to the Southernmost transect line. *Tetraria Thermalis* clusters were all located west of the wetland. Of all the species, the *Platycaulos Compressus* was the most dominant in the wetland and surrounding portions of the Steenbras reserve.

Conclusions

This study presented a methodology for using multispectral aerial photography to discriminate several wetland plant families and species. The study found that the Normalized Green–Red Difference Index (NGRDI) and Red Green Vegetation Index (RG) were the most critical indices for the discrimination of the different wetland plant species at the start of summer. The other chlorophyll and water-sensitive indices were also essential for classifying the plant species. It was also found that classifying a subset of indices and bands produced overall accuracies of between 87.4% and 83.6% and kappa hat accuracies of 0.85 and 0.81. The accuracy of the classification models improved by up to 3.7% after combining selected vegetation indices and band data, and the overall classification accuracy of all three classifications by between 0.4% and 1.6%.

Of the three classifiers, Random Forest performed best, with an overall accuracy of 87% and kappa hat of 0.85. It was followed by Support Vector Machines and then K Nearest Number. However, K Nearest Neighbour performed well when classifying the *Erica* family of flowering plants and the small plant clusters of *Borbotia Gladiata, Dead Platycaulos Compressus* and *Restio Dispar.Grubbia Rosmarinifolia* and *Platycaulos Compressus* were the most notable species in the northern and wettest portion of the wetland. The *Ericaceae* species were spread around the drier parts of the wetland. *Elegia Mucronata, Berzelia Lanuginosa*, *Berzelia Alopecuroides* and *Tetraria Thermalis* thrived in the wetland's moist soils at the centre and western regions. *Borbotia Gladiata* and *Restio Dispar* occurred in tiny clusters in the wetland on dry patches.

This study used UAV multispectral aerial photography to classify plant species in a wetland in the Fynbos Biome. To our knowledge, no study has tested the viability of using remote sensing data to map wetland species in the Proteaceae, Iridaceae, Restionaceae, Ericaceae, Asteraceae and Cyperaceae families. The results show that the methodology used in this study could be replicated in other Fynbos wetlands. Future studies should explore classifications of the same species in different seasons to assess the best time of year to classify them. In addition, future studies should explore the use of Geographic Object-Based Image Analysis and deep learning classifiers.

There are significant benefits and implications of this pioneering study. Firstly, the study contributes to the spectral characterisation of wetland plant species in the Fynbos Biome. It provides the foundation for future Fynbos remote sensing research and practical implications for conservation and land management. Moreover, understanding the distribution and spatial preferences of key wetland species can assist conservation managers in making more informed decisions about land use and protection strategies in the Cape Floristic Region. Thus, this knowledge will contribute to preserving these vital wetland ecosystems and their ecological functions.

Acknowledgements We would like to thank the City of Cape Town for granting us permission to conduct the research in the Steenbras reserve. Thanks also to Douglas Euston-Brown for his assistance in identifying the plant species. We are grateful for feedback from the anonymous reviewers which improved the quality of the manuscript.

Author contributions Conceptualization, KM, TD and JS; methodology, KM; software, KM; validation, KM, TD and JS; formal analysis, KM; investigation, KM; resources, JS; data curation, KM; writing—original draft preparation, KM; writing—review and editing, KM; visualization, KM; supervision, TD; project administration, MS; All authors have read and agreed to the published version of the manuscript.

Funding Open access funding provided by University of Cape Town.

Data availability The data used in this study is available upon request from the authors.

Declarations

Competing interests The authors declare no competing interests.

References

Abeysinghe T, Simic Milas A, Arend K et al (2019) Mapping invasive phragmites australis in the old woman Creek Estuary using UAV remote sensing and machine learning classifiers. Remote Sens 11:1380. https://doi.org/10.3390/rs11111380

Adam E, Mutanga O, Rugege D (2010) Multispectral and hyperspectral remote sensing for identification and mapping of wetland vegetation: a review. Wetl Ecol Manag 18:281–296. https://doi.org/10.1007/s11273-009-9169-z

Adamus PR (1992) Choices in monitoring wetlands. In: McKenzie DH, Hyatt DE, V.J. M (eds) Ecological indicators. Springer US, Boston, MA, pp 571–592

Allen N, Cooksley H, Buchmann C et al (2001) Automated mapping and identification of shrub individuals in South Africa's Fynbos biome using drone imagery and deep learning. In: Mosch C, Salk J, Wagner FW (eds) 7th bwHPC Symposium. Universität Ulm, Ulm, pp 11–16

Alvarez-Vanhard E, Corpetti T, Houet T (2021) UAV & satellite synergies for optical remote sensing applications: a literature review. Sci Remote Sens 3:100019. https://doi.org/10.1016/j.srs.2021.100019

Arun S (2022) Principal component analysis (Pca) in the evaluation of vegetation indices derived from time-series remote sensing data: a review. Int J Creat Res Thought 10:955–965

Assmann JJ, Kerby JT, Cunliffe AM, Myers-Smith IH (2019) Vegetation monitoring using multispectral sensors—best practices and lessons learned from high latitudes. J Unmanned Veh Syst 7:54–75. https://doi.org/10.1139/juvs-2018-0018

Avola G, Di Gennaro SF, Cantini C et al (2019) Remotely sensed vegetation indices to discriminate field-grown olive cultivars. Remote Sens 11:1242. https://doi.org/10.3390/rs11101242

Bannari A, Asalhi H, Teillet PM (2002) Transformed difference vegetation index (TDVI) for vegetation cover mapping. IEEE International Geoscience and Remote Sensing Symposium. IEEE, Toronto, pp 3053–3055

Bassi D, Menossi M, Mattiello L (2018) Nitrogen supply influences photosynthesis establishment along the sugarcane leaf. Sci Rep 8:2327. https://doi.org/10.1038/s41598-018-20653-1

Belgiu M, Drăguţ L (2016) Random forest in remote sensing: a review of applications and future directions. ISPRS J Photogrammetry Remote Sens 114:24–31. https://doi.org/10.1016/j.isprsjprs.2016.01.011

Bhatnagar S, Gill L, Regan S et al (2020) Mapping Vegetation communities inside wetlands using SENTINEL-2 imagery in Ireland. Int J Appl Earth Obs Geoinf 88:102083. https://doi.org/10.1016/j.jag.2020.102083

Blake D, Hartnady C, Hay R, Riemann K (2021) Geoethics of Bulk Groundwater Abstraction in an Ecologically Sensitive Area: Steenbras Wellfield (Cape Town). Advances in Geoethics and Groundwater Management: Theory and Practice for a Sustainable Development: Proceedings of the 1st Congress on Geoethics and Groundwater Management (GEOETH\&GWM'20). Springer, Porto, pp 429–432

Blewitt G (2015) GPS and Space-Based Geodetic Methods. In: Schubert G (ed) Treatise on Geophysics, 2nd edn. Elsevier, Amsterdam, pp 307–338

Boiarskii B, Hasegawa H (2019) Comparison of NDVI and NDRE indices to detect differences in Vegetation and Chlorophyll Content. J Mech Continua Math Sci spl1:20–29. https://doi.org/10.26782/jmcms.spl.4/2019.11.00003

Bonthuys J (2020) Nature-based solutions for the future: securing wetlands for water security in the Western Cape. Water Wheel 19:32–35

Boon MA, Greenfield R, Tesfamichael S (2016) Wetland assessment using unmanned aerial vehicle (UAV) photogrammetry. International archives of the photogrammetry, remote sensing and spatial Information sciences. ISPRS Archives 41:781–788. https://doi.org/10.5194/isprsarchives-XLI-B1-781-2016

Breiman L (1996) Bagging predictors. Mach Learn 24:123–140

Chen J (1996) Evaluation of Vegetation indices and a modified simple ratio for Boreal Applications. Can J Remote Sens 22:229–242. https://doi.org/10.1080/07038992.1996.10855178

Chen R-C, Dewi C, Huang S-W, Caraka RE (2020) Selecting critical features for data classification based on machine learning methods. J Big Data 7:52. https://doi.org/10.1186/s40537-020-00327-4

Cheng G, Han J (2016) A survey on object detection in optical remote sensing images. ISPRS J Photogrammetry Remote Sens 117:11–28. https://doi.org/10.1016/j.isprsjprs.2016.03.014

Chirici G, Mura M, McInerney D et al (2016) A meta-analysis and review of the literature on the k-Nearest neighbors technique for forestry applications that use remotely sensed data. Remote Sens Environ 176:282–294. https://doi.org/10.1016/j.rse.2016.02.001

Choudhary SS, Biswal S, Saha R, Chatterjee C (2021) A non-destructive approach for assessment of nitrogen status of wheat crop using unmanned aerial vehicle equipped with RGB camera. Arab J Geosci 14:1739. https://doi.org/10.1007/s12517-021-08139-3

Congalton R, Oderwald R, Mead R (1983) Assessing landsat classification accuracy using discrete multivariate analysis statistical techniques. Photogramm Eng Remote Sensing 49:1671–1678

DeLancey ER, Simms JF, Mahdianpari M et al (2019) Comparing deep learning and shallow learning for large-scale wetland classification in Alberta, Canada. Remote Sens 12:2. https://doi.org/10.3390/rs12010002

De Roeck E, Miya M, Verhoest N et al (2007) Integrating remote sensing and wetland ecology: A case study on South African wetlands. Proceedings of MultiTemp 2007 - 2007 International Workshop on the Analysis of Multi-Temporal Remote Sensing Images. IEEE, Leuven, Belgium

Demarchi L, Kania A, Ciężkowski W et al (2020) Recursive feature elimination and Random Forest Classification of Natura 2000 Grasslands in Lowland River Valleys of Poland based on Airborne Hyperspectral and LiDAR Data Fusion. Remote Sens (Basel) 12:1842. https://doi.org/10.3390/rs12111842

Doughty CL, Cavanaugh KC (2019) Mapping coastal wetland biomass from high resolution unmanned aerial vehicle (UAV) imagery. Remote Sens 11:540. https://doi.org/10.3390/rs11050540

Dronova I, Kislik C, Dinh Z, Kelly M (2021) A review of unoccupied aerial vehicle use in Wetland Applications. Drones 5:45. https://doi.org/10.3390/drones5020045

Du B, Mao D, Wang Z et al (2021) Mapping Wetland Plant communities using unmanned aerial vehicle hyperspectral imagery by comparing Object/Pixel-Based classifications combining multiple machine-learning algorithms. IEEE J Sel Top Appl Earth Obs Remote Sens 14:8249–8258. https://doi.org/10.1109/JSTARS.2021.3100923

Dumakude N, Graham M (2017) Assessing wetland health using a newly developed land cover citizen science tool for use by local people who are not wetland specialists. South Afr J Environ Educ 33:71. https://doi.org/10.4314/sajee.v.33i1.6

Duncan P, Podest E, Esler KJ et al (2023) Mapping Invasive Herbaceous Plant species with Sentinel-2 Satellite Imagery: Echium plantagineum in a Mediterranean Shrubland as a case study. Geomatics 3:328–344. https://doi.org/10.3390/geomatics3020018

Elazab A, Ordóñez RA, Savin R et al (2016) Detecting interactive effects of N fertilization and heat stress on maize productivity by remote sensing techniques. Eur J Agron 73:11–24. https://doi.org/10.1016/j.eja.2015.11.010

Elliott R (2014) Geographic information systems (GIS) and libraries: concepts, services and resources. Libr Hi Tech News 31:8–11. https://doi.org/10.1108/LHTN-07-2014-0054

Everitt JH, Yang C, Escobar DE et al (2002) Reflectance characteristics and remote sensing of a riparian zone in South Texas. Southwest Nat 47:433. https://doi.org/10.2307/3672500

Ferrer-González E, Agüera-Vega F, Carvajal-Ramírez F, Martínez-Carricondo P (2020) UAV photogrammetry accuracy assessment for corridor mapping based on the number and distribution of ground control points. Remote Sens 12:2447. https://doi.org/10.3390/RS12152447

Gallant A (2015) The challenges of Remote Monitoring of wetlands. Remote Sens (Basel) 7:10938–10950. https://doi.org/10.3390/rs70810938

Gausman HW (1977) Reflectance of leaf components. Remote Sens Environ 6:1–9. https://doi.org/10.1016/0034-4257(77)90015-3

Gibril MBA, Kalantar B, Al-Ruzouq R et al (2020) Mapping heterogeneous urban landscapes from the Fusion of Digital Surface Model and Unmanned Aerial vehicle-based images using adaptive Multiscale Image Segmentation and classification. Remote Sens (Basel) 12:1081. https://doi.org/10.3390/rs12071081

Giglio M, De, Greggio N, Goffo F et al (2019) Comparison of pixel- and object-based classification methods of unmanned aerial vehicle data applied to coastal dune vegetation communities: Casal Borsetti case study. Remote Sens (Basel) 11:1–21. https://doi.org/10.3390/rs11121416

Gitelson AA (2005) Remote estimation of canopy chlorophyll content in crops. Geophys Res Lett 32:L08403. https://doi.org/10.1029/2005GL022688

Gitelson AA (2011) Non-destructive estimation of Foliar Pigment (chlorophylls, carotenoids and anthocyanins) contents: evaluating a Semianalytical three-band model. In: Thenkabail P, Lyon J, Huete A (eds) Hyperspectral Remote Sensing of Vegetation. Taylor and Francis, Boca Raton, Florida, pp 141–165
Gitelson AA, Kaufman YJ, Stark R, Rundquist D (2002) Novel algorithms for remote estimation of vegetation fraction. Remote Sens Environ 80:76–87. https://doi.org/10.1016/S0034-4257(01)00289-9
Goel NS, Qin W (1994) Influences of canopy architecture on relationships between various vegetation indices and LAI and fpar: a computer simulation. Remote Sens Reviews 10:309–347. https://doi.org/10.1080/02757259409532252
Govender M, Dye P, Weiersbye IM et al (2009) Review of commonly used remote sensing and ground-based technologies to measure plant water stress. Water SA 35:741–752. https://doi.org/10.4314/wsa.v35i5.49201
Han M, Pan B, Liu Y, Bin et al (2019) Wetland biomass inversion and space differentiation: a case study of the Yellow River Delta Nature Reserve. PLoS ONE 14:e0210774. https://doi.org/10.1371/journal.pone.0210774
Harvey KR, Hill GJE (2001) Vegetation mapping of a tropical freshwater swamp in the Northern Territory, Australia: a comparison of aerial photography, landsat TM and SPOT satellite imagery. Int J Remote Sens 22:2911–2925
Hasan I, Liu W, Xu C (2023) Monitoring and analyzing the Seasonal Wetland Inundation Dynamics in the Everglades from 2002 to 2021 using Google Earth Engine. Geographies 3:161–177. https://doi.org/10.3390/geographies3010010
Hemati M, Hasanlou M, Mahdianpari M, Mohammadimanesh F (2023) Iranian wetland inventory map at a spatial resolution of 10 m using Sentinel-1 and Sentinel-2 data on the Google Earth Engine cloud computing platform. Environ Monit Assess 195:558. https://doi.org/10.1007/s10661-023-11202-z
Higgisson W, Cobb A, Tschierschke A, Dyer F (2021) Estimating the cover of Phragmites australis using unmanned aerial vehicles and neural networks in a semi-arid wetland. River Res Appl 37:1312–1322. https://doi.org/10.1002/rra.3832
Hunt ER, Cavigelli M, Daughtry CST et al (2005) Evaluation of digital photography from model aircraft for remote sensing of crop biomass and nitrogen status. Precis Agric 6:359–378. https://doi.org/10.1007/s11119-005-2324-5
Islam MK, Simic Milas A, Abeysinghe T, Tian Q (2023) Integrating UAV-Derived information and worldview-3 imagery for mapping wetland plants in the old woman Creek Estuary, USA. Remote Sens 15:1090. https://doi.org/10.3390/rs15041090
Jafarzadeh H, Mahdianpari M, Gill EW, et al (2022) Remote sensing and machine learning tools to support wetland monitoring: a meta-analysis of three decades of research. Remote Sens 14:6104. https://doi.org/10.3390/rs14236104
Janiesch C, Zschech P, Heinrich K (2021) Machine learning and deep learning. Elect Mark 31:685–695. https://doi.org/10.1007/s12525-021-00475-2
Jannoura R, Brinkmann K, Uteau D et al (2015) Monitoring of crop biomass using true colour aerial photographs taken from a remote controlled hexacopter. Biosyst Eng 129:341–351. https://doi.org/10.1016/j.biosystemseng.2014.11.007
Jeanneret C, Rambaldi G (2016) Series: ICTs for agriculture Drone Governance A Scan of Policies, Laws and Regulations Governing the Use of Unmanned Aerial Vehicles (UAVs) in 79 ACP Countries. Wageningen
Jia M, Mao D, Wang Z et al (2020) Tracking long-term floodplain wetland changes: a case study in the China side of the Amur River Basin. Int J Appl Earth Obs Geoinf 92:102185. https://doi.org/10.1016/j.jag.2020.102185
Jiang Z, Huete A, Didan K, Miura T (2008) Development of a two-band enhanced vegetation index without a blue band. Remote Sens Environ 112:3833–3845. https://doi.org/10.1016/j.rse.2008.06.006
Jin Y, Sung S, Lee D et al (2016) Mapping Deforestation in North Korea using phenology-based Multi-index and Random Forest. Remote Sens (Basel) 8:997. https://doi.org/10.3390/rs8120997
Job N, Mbona N, Dayaram A, Kotze D (2018) Guidelines for mapping wetlands in South Africa. Pretoria
Jovic A, Brkic K, Bogunovic N (2015) A review of feature selection methods with applications. 2015 38th International Convention on Information and Communication Technology, Electronics and Microelectronics (MIPRO). IEEE, Opatija, pp 1200–1205
Kaplan E, Hegarty C (2017) Understanding GPS/GNSS: principles and applications, 3rd edn. Artech, Boston
Karabulut M (2018) An examination of Spectral Reflectance properties of some Wetland Plants in Göksu Delta, Turkey. J Int Environ Application Sci 13:194–203
Karasiak N (2016) Dzetsaka Qgis Classification plugin
Kingsford RT, Basset A, Jackson L (2016) Wetlands: conservation's poor cousins. Aquat Conserv 26:892–916. https://doi.org/10.1002/aqc.2709
Klemas V (2013) Remote sensing of Coastal Wetland Biomass: an overview. J Coast Res 290:1016–1028. https://doi.org/10.2112/JCOASTRES-D-12-00237.1
Kranjčić N, Medak D (2020) Evaluating different machine learning methods on rapideye and planetscope satellite imagery. Geodetski List 74:1–18
Kuradusenge M, Hitimana E, Hanyurwimfura D et al (2023) Crop yield prediction using machine learning models: case of Irish potato and maize. Agriculture 13:225. https://doi.org/10.3390/agriculture13010225
Lane C, Liu H, Autrey B et al (2014) Improved Wetland classification using eight-Band High Resolution Satellite Imagery and a Hybrid Approach. Remote Sens (Basel) 6:12187–12216. https://doi.org/10.3390/rs61212187
Lane CR, Anenkhonov O, Liu H et al (2015) Classification and inventory of freshwater wetlands and aquatic habitats in the Selenga River Delta of Lake Baikal, Russia, using high-resolution satellite imagery. Wetl Ecol Manag 23:195–214. https://doi.org/10.1007/s11273-014-9369-z
Li W, Niu Z, Chen H et al (2016) Remote estimation of canopy height and aboveground biomass of maize using high-resolution stereo images from a low-cost unmanned aerial vehicle system. Ecol Indic 67:637–648. https://doi.org/10.1016/j.ecolind.2016.03.036

Li G, Wu J, Zhao C, Tian Y (2017) Double differencing within GNSS constellations. GPS Solutions 21:1161–1177. https://doi.org/10.1007/s10291-017-0599-4

Liu D, Xia F (2010) Assessing object-based classification: advantages and limitations. Remote Sens Lett 1:187–194. https://doi.org/10.1080/01431161003743173

Louhaichi M, Borman MM, Johnson DE (2001) Spatially located platform and aerial photography for documentation of grazing impacts on wheat. Geocarto Int 16:65–70. https://doi.org/10.1080/10106040108542184

Ma L, Fu T, Blaschke T et al (2017) Evaluation of feature selection methods for object-based land cover mapping of unmanned aerial vehicle imagery using random forest and support vector machine classifiers. ISPRS Int J Geo-inf 6:51. https://doi.org/10.3390/ijgi6020051

Ma S, Zhou Y, Gowda PH et al (2019) Application of the water-related spectral reflectance indices: a review. Ecol Indic 98:68–79. https://doi.org/10.1016/j.ecolind.2018.10.049

Maciuk K (2018) Advantages of combined GNSS Processing Involving a limited number of visible satellites. Sci J Silesian Univ Technol Ser Transp 98:89–99. https://doi.org/10.20858/sjsutst.2018.98.9

Martínez-Carricondo P, Agüera-Vega F, Carvajal-Ramírez F et al (2018) Assessment of UAV-photogrammetric mapping accuracy based on variation of ground control points. Int J Appl Earth Obs Geoinf 72:1–10. https://doi.org/10.1016/j.jag.2018.05.015

Mas J-F, García-Álvarez D, Paegelow M et al (2022) Metrics based on a Cross-tabulation Matrix to Validate Land Use Cover maps. Land Use Cover datasets and Validation Tools. Springer International Publishing, Cham, pp 127–151

McFeeters SK (1996) The use of the normalized difference Water Index (NDWI) in the delineation of open water features. Int J Remote Sens 17:1425–1432. https://doi.org/10.1080/01431169608948714

Millar JB (1973) Estimation of area and circumference of small wetlands. J Wildl Manage 37:30–38. https://doi.org/10.2307/3799735

Mirmazloumi SM, Moghimi A, Ranjgar B et al (2021) Status and trends of Wetland studies in Canada using Remote Sensing Technology with a focus on Wetland classification: a bibliographic analysis. Remote Sens (Basel) 13:4025. https://doi.org/10.3390/rs13204025

Mishra NB (2020) Wetlands: Remote Sensing. Wetlands and Habitats, 2nd edn. CRC Press, Boca Raton, pp 201–212

Moity N, Delgado B, Salinas-de-leo P (2019) Mangroves in the Galapagos islands: distribution and dynamics. PLoS ONE 14:1–35. https:. //doi.org/

Montgomery J, Mahoney C, Brisco B et al (2021) Remote sensing of wetlands in the Prairie Pothole Region of North America. Remote Sens (Basel) 13:3878. https://doi.org/10.3390/rs13193878

Morrison LW (2021) Nonsampling error in vegetation surveys: understanding error types and recommendations for reducing their occurrence. Plant Ecol 222:577–586. https://doi.org/10.1007/s11258-021-01125-5

Morrison LW, Bingham SN, Young CC (2020) Inter-observer Error in Wetland Vegetation surveys. Wetlands 40:249–258. https://doi.org/10.1007/s13157-019-01173-8

Motohka T, Nasahara KN, Oguma H, Tsuchida S (2010) Applicability of Green-Red Vegetation Index for Remote sensing of vegetation phenology. Remote Sens (Basel) 2:2369–2387. https://doi.org/10.3390/rs2102369

Mucherino A, Papajorgji PJ, Pardalos PM (2009a) k-Nearest neighbor classification. Data Mining in Agriculture. Springer optimization and its applications 34. Springer, New York, pp 83–106

Mucherino A, Papajorgji PJ, Pardalos PM (2009b) Support Vector Machines. Data Mining in Agriculture, 34th edn. Springer, New York, pp 123–141

Mudereri BT, Dube T, Niassy S et al (2020) Is it possible to discern Striga weed (Striga hermonthica) infestation levels in maize agro-ecological systems using in-situ spectroscopy? Int J Appl Earth Obs Geoinf. https://doi.org/10.1016/j.jag.2019.102008

Ndlovu HS, Odindi J, Sibanda M et al (2021) A Comparative Estimation of Maize Leaf Water Content Using Machine Learning Techniques and unmanned aerial vehicle (UAV)-Based proximal and remotely sensed data. Remote Sens (Basel) 13:4091. https://doi.org/10.3390/rs13204091

Nezami S, Khoramshahi E, Nevalainen O et al (2020) Tree species classification of Drone Hyperspectral and RGB Imagery with Deep Learning Convolutional neural networks. Remote Sens (Basel) 12:1070. https://doi.org/10.3390/rs12071070

Nikolakopoulos KG, Vaiopoulos DA, Skianis GA (2004) Use of vegetation indexes and PCA method with remote sensing data for the classification of burnt areas according to how many times they have been burnt. In: Owe M, Guido D, Moreno JF, Calera A (eds) Remote Sensing for Agriculture, Ecosystems, and Hydrology V. Proc.SPIE, Barcelona, pp 196–207

Ollis D, Snaddon K, Job N, Mbona N (2013) Classification system for wetlands and other aquatic ecosystems in South Africa: user Manual: Inland systems, SANBI Biod. South African National Biodiversity Institute, Pretoria

Padró J-C, Carabassa V, Balagué J et al (2019) Monitoring opencast mine restorations using Unmanned Aerial System (UAS) imagery. Sci Total Environ 657:1602–1614. https://doi.org/10.1016/j.scitotenv.2018.12.156

Patel N, Kaushal B (2010) Improvement of user's accuracy through classification of principal component images and stacked temporal images. Geo-spatial Inform Sci 13:243–248. https://doi.org/10.1007/s11806-010-0380-0

Pedregosa F, Varoquaux G, Gramfort A et al (2011) Scikit-learn: machine learning in Python. J Mach Learn Res 12:2825–2830

Poncet AM, Knappenberger T, Brodbeck C et al (2019) Multispectral UAS Data Accuracy for different Radiometric calibration methods. Remote Sens (Basel) 11:1917. https://doi.org/10.3390/rs11161917

Poona NK, van Niekerk A, Nadel RL, Ismail R (2016) Random Forest (RF) wrappers for Waveband Selection and classification of Hyperspectral Data. Appl Spectrosc 70:322–333. https://doi.org/10.1177/0003702815620545

Ramezan CA (2022) Transferability of recursive feature elimination (RFE)-Derived feature sets for support

Vector Machine Land Cover classification. Remote Sens 14:6218. https://doi.org/10.3390/rs14246218
Ramsey Elijah I, Rangoonwala A, Middleton B, Lu Z (2009) Satellite optical and radar data used to track wetland forest impact and short-term recovery from Hurricane Katrina. Wetlands 29:66–79. https://doi.org/10.1672/08-103.1
Rasmussen J, Ntakos G, Nielsen J et al (2016) Are vegetation indices derived from consumer-grade cameras mounted on UAVs sufficiently reliable for assessing experimental plots? Eur J Agron 74:75–92. https://doi.org/10.1016/j.eja.2015.11.026
Rebelo LM, Finlayson CM, Nagabhatla N (2009) Remote sensing and GIS for wetland inventory, mapping and change analysis. J Environ Manage 90:2144–2153. https://doi.org/10.1016/j.jenvman.2007.06.027
Rezaee M, Mahdianpari M, Zhang Y, Salehi B (2018) Deep convolutional neural network for Complex Wetland classification using Optical Remote sensing imagery. IEEE J Sel Top Appl Earth Obs Remote Sens 11:3030–3039. https://doi.org/10.1109/JSTARS.2018.2846178
Richardson AJ, Wiegand CL (1977) Distinguishing vegetation from soil background information. Photogramm Eng Remote Sensing 43:1541–1552
Roujean J-L, Breon F-M (1995) Estimating PAR absorbed by vegetation from bidirectional reflectance measurements. Remote Sens Environ 51:375–384. https://doi.org/10.1016/0034-4257(94)00114-3
Rouse JW, Haas RH, Schell JA et al (1974) Monitoring vegetation systems in the Great Plains with ERTS. NASA Spec Publ 351:309
Rundquist DC, Narumalani S, Narayanan RM (2001) A review of wetlands remote sensing and defining new considerations. Remote Sens Reviews 20:207–226. https://doi.org/10.1080/02757250109532435
Rwanga SS, Ndambuki JM (2017) Accuracy Assessment of Land Use/Land Cover classification using remote sensing and GIS. Int J Geosci 08:611–622. https://doi.org/10.4236/ijg.2017.84033
Sharp MJ, Keddy PA (1986) A quantitative technique for estimating the boundaries of wetlands from vegetation data. Environ Manage 10:107–112. https://doi.org/10.1007/BF01866422
Sheykhmousa M, Mahdianpari M, Ghanbari H et al (2020) Support Vector Machine Versus Random Forest for Remote sensing image classification: a Meta-analysis and systematic review. IEEE J Sel Top Appl Earth Obs Remote Sens 13:6308–6325. https://doi.org/10.1109/JSTARS.2020.3026724
Sica YV, Quintana RD, Radeloff VC, Gavier-pizarro GI (2016) Science of the Total Environment Wetland loss due to land use change in the Lower Paraná River Delta, Argentina. Sci Total Environ J 568:967–978. https://doi.org/10.1016/j.scitotenv.2016.04.200
Smigaj M, Gaulton R, Suárez JC, Barr SL (2019) Combined use of spectral and structural characteristics for improved red band needle blight detection in pine plantation stands. For Ecol Manage 434:213–223. https://doi.org/10.1016/j.foreco.2018.12.005
Song B, Park K (2020) Detection of aquatic plants using multispectral UAV Imagery and Vegetation Index. Remote Sens 12:387. https://doi.org/10.3390/rs12030387
Sripada RP, Heiniger RW, White JG, Weisz R (2005) Aerial Color Infrared Photography for determining late-season Nitrogen requirements in Corn. Agron J 97:1443–1451. https://doi.org/10.2134/agronj2004.0314
Stöcker C, Bennett R, Nex F et al (2017) Review of the current state of UAV regulations. Remote Sens 9:459. https://doi.org/10.3390/rs9050459
Story M, Congalton RG (1986) Remote sensing brief Accuracy Assessment: a user's perspective. Photogramm Eng Remote Sensing 52:397–399
Sun S, Wang Y, Song Z et al (2021) Modelling aboveground biomass carbon stock of the bohai rim coastal wetlands by integrating remote sensing, terrain, and climate data. Remote Sens 13:1–16. https://doi.org/10.3390/rs13214321
Tang J, Alelyani S, Liu H (2014) Feature selection for classification: a review. In: Aggarwal CC, Kong X, Gu Q et al (eds) Data classification: algorithms and applications. Chapman and Hall/CRC, Boca Raton, pp 571–605
Thanh Noi P, Kappas M (2017) Comparison of Random Forest, k-Nearest neighbor, and support Vector Machine classifiers for Land Cover classification using Sentinel-2 imagery. Sensors 18:18. https://doi.org/10.3390/s18010018
Tian Y, Jia M, Wang Z et al (2020) Monitoring Invasion process of Spartina alterniflora by Seasonal Sentinel-2 imagery and an object-based Random Forest classification. Remote Sens 12:1383. https://doi.org/10.3390/rs12091383
Tu YH, Johansen K, Phinn S, Robson A (2019) Measuring canopy structure and condition using multi-spectral UAS imagery in a horticultural environment. Remote Sens 11:15–17. https://doi.org/10.3390/rs11030269
Tucker CJ (1979) Red and photographic infrared linear combinations for monitoring vegetation. Remote Sens Environ 8:127–150. https://doi.org/10.1016/0034-4257(79)90013-0
Ulvi A (2021) The effect of the distribution and numbers of ground control points on the precision of producing orthophoto maps with an unmanned aerial vehicle. J Asian Archit Building Eng 20:806–817. https://doi.org/10.1080/13467581.2021.1973479
van Blerk JJ, West AG, Smit J et al (2022) UAVs improve detection of seasonal growth responses during post-fire shrubland recovery. Landsc Ecol 37:3179–3199. https://doi.org/10.1007/s10980-022-01535-4
Van Deventer H, Smith-Adao L, Petersen C et al (2018) Review of available data for a South African inventory of Inland aquatic ecosystems (SAIIAE). Water SA 44:184–199. https://doi.org/10.4314/wsa.v44i2.05
Van Sickle J (2015) GPS for Land surveyors, 4th edn. CRC Press, Boca Raton
Veljanovski T, Kanjir U, Oštir K (2011) Object-based image analysis of remote sensing data. Geodetski Vestnik 55:641–688
Wang Y, Wang D, Shi P, Omasa K (2014) Estimating rice chlorophyll content and leaf nitrogen concentration with a

digital still color camera under natural light. Plant Methods 10:36. https://doi.org/10.1186/1746-4811-10-36
Whiteside T, Ahmad W (2005) A Comparison of Object-Oriented and Pixel-Based Classification Methods for Mapping Land Cover in Northern Australia. Proceedings of SSC2005 Spatial intelligence innovation and praxis The national biennial Conference of the Spatial Sciences Institute. Spatial Sciences Institute, Canberra, pp 1225–1231
Wiese J-L, Finkelstein J, Milandri SG (2020) City of Cape Town New Water Programme. Civil Eng = Siviele Ingenieurswese 28:39–45. https://doi.org/10.10520/ejc-civeng-v28-n7-a10
Wijana N, Setiawan IGAN (2020) Mapping and Distribution of Useful Plant Species in Bukit Kangin Forest, Pegringsingan Village, Karangasem, Bali. Proceedings of the 3rd International Conference on Innovative Research Across Disciplines (ICIRAD 2019). Atlantis Press, Paris
Wijesingha SJ (2020) Fine-scale grassland monitoring using unmanned aerial vehicle borne remote sensing. University of Kassel, Germany
Windle AE, Staver LW, Elmore AJ et al (2023) Multi-temporal high-resolution marsh vegetation mapping using unoccupied aircraft system remote sensing and machine learning. Front Remote Sens 4:1140999. https://doi.org/10.3389/frsen.2023.1140999
Wittridge H-M (2011) Integrated reserve management plansteenbras nature reserve. Cape Town
Xu T, Weng B, Yan D et al (2019) Wetlands of International Importance: Status, threats, and Future Protection. Int J Environ Res Public Health 16:1818. https://doi.org/10.3390/ijerph16101818
Yan F, Liu X, Chen J et al (2017) China's wetland databases based on remote sensing technology. Chin Geogr Sci 27:374–388. https://doi.org/10.1007/s11769-017-0872-z
Yang G, Liu J, Zhao C et al (2017) Unmanned aerial vehicle remote sensing for field-based crop phenotyping: Current status and perspectives. Front Plant Sci 8:1111. https://doi.org/10.3389/fpls.2017.01111
Yang R, Luo F, Ren F et al (2022) Identifying Urban wetlands through Remote sensing scene classification using deep learning: a case study of Shenzhen, China. ISPRS Int J Geoinf 11:131. https://doi.org/10.3390/ijgi11020131
Zhu H, Huang Y, Li Y et al (2022) Predicting plant diversity in beach wetland downstream of Xiaolangdi reservoir with UAV and satellite multispectral images. Sci Total Environ 819:153059. https://doi.org/10.1016/j.scitotenv.2022.153059
Zhuo W, Wu N, Shi R, Wang Z (2022) UAV mapping of the chlorophyll content in a tidal flat wetland using a combination of spectral and frequency indices. Remote Sens 14:827. https://doi.org/10.3390/rs14040827

Publisher's Note Springer Nature remains neutral with regard to jurisdictional claims in published maps and institutional affiliations.